Electrochemical Characterization of $PrBa_{2-x}Sr_xCu_3O_{6+\delta}$ Layered Oxides as Innovative and Efficient Oxygen Electrode for IT-SOFCs

Giulio Cordaro[a,b], Aurélien Flura[c], Alessandro Donazzi[a], Renato Pelosato[d], Fabrice Mauvy[c], Cinzia Cristiani[b], Giovanni Dotelli[b], Jean-Claude Grenier[c]*

[a]Dipartimento di Energia, Politecnico di Milano, Via Lambruschini 4, 20156 Milano, Italy

[b]Dipartimento di Chimica Materiali e Ingegneria Chimica "G. Natta", Politecnico di Milano, Piazza Leonardo da Vinci 32, 20133 Milano, Italy

[c]Institut de Chimie de la Matière Condensée de Bordeaux (ICMCB), UMR 7315, CNRS, Université de Bordeaux, 87 Av. Dr Schweitzer, F-33608 Pessac Cedex, France

[d]INSTM R.U. and Università di Bergamo, Dipartimento di Ingegneria, Viale Marconi 5, 24044 Dalmine (BG), Italy

*corresponding author:
Giulio Cordaro
Dipartimento di Energia
Via Lambruschini 4, 20156 Milano (Italy)
Phone: 0039 02 2399 8685
Fax: 0039 02 2399 8566
e-mail: giulio.cordaro@polimi.it

Abstract

$PrBa_2Cu_3O_{6+\delta}$ (P or Pr123) and $PrBa_{1.5}Sr_{0.5}Cu_3O_{6+\delta}$ (PS) layered perovskite-type oxides are synthesized and characterized as oxygen electrodes in IT-SOFCs. The layered structure of P and PS compounds is constituted by the regular alternation along the crystallographic c axis of Pr-O planes, Cu^{2+} chains (CN = 4) and Cu^{3+} pyramidal (CN = 5) layers. The absence of cobalt, the presence of aliovalent cations and large amounts of oxygen vacancies generated interest about the investigation of the electrochemical properties of the Pr123 peculiar structure. A 25% Ba substitution with Sr is evaluated in order to improve the electronic conductivity of the undoped material. The compounds are synthesized via molten citrate procedure and characterized by XRPD, 4-probe conductivity measurements (100-800 °C) and EIS tests on symmetric cells in air varying the temperature (450-850 °C). SEM images of *post mortem* cells are collected to evaluate the adhesion between components, layers thickness and particle morphology. Sr doping does not significantly improve the electrical conductivity, but P sample present a considerable hysteresis between values measured during cooling and heating ramps. Conductivity values are lower than 100 S/cm, but no electrical limitations are observed in EIS results. The introduction of a thin PrDC interlayer greatly reduces the resistances for both the compounds and the 0.15 $\Omega \cdot cm^2$ target is almost fulfilled at 600 °C (0.17 $\Omega \cdot cm^2$ for PS+PrDC sample).

Keywords: Pr123, Layered Perovskite, Cathode, Oxygen Electrode, IT-SOFC, EIS

1. Introduction

The *RE*$Ba_2Cu_3O_{6+\delta}$ (*RE* = Rare Earth) family of solid oxides has widely been studied since 1986, when Bednorz and Muller [1] discovered high temperature superconductivity in La-Ba-Cu-O system. The following year Wu et al. [2] discovered a critical temperature of 93 K in $YBa_2Cu_3O_{6+\delta}$ (YBCO or Y123), which became the first material produced with a T_C above liquid nitrogen boiling point (77 K). The substitution of Y with other *RE*s did not show remarkable changes in the T_C, if the 1:2:3 structure was preserved. The introduction of Pr was the only exception, which seemed to suppress the superconductivity, although leading to the formation of the Pr123 phase. Conversely, Blackstead et al. [3] observed inhomogeneous granular superconductivity in both films and powders of Pr123, suggesting that only perfect $PrBa_2Cu_3O_7$ crystals superconduct in the proximity of the Cu-O chains. Zou et al. [4] confirmed this result, growing single crystals by the travelling-solvent floating-zone (TSFZ) method in oxygen-reduced atmosphere. Some years later, Dow and Harshman [5] tried to demonstrate that Ba-O planes contain the superconductivity, contradicting the previously accepted belief that Cu-O chains were the responsible features [6]. These anomalous behaviours attracted the attention of many researchers who tried to explain the superconductivity suppression by disparate theories. According to the work of Fehrenbaher and Rice [7], the reason was the local Pr(*4f*)-O(*2p*) hybridization state which binds holes to Pr sites with strength depending on the Pr-O distance. This assumption was first supported by experimental results showing a dependence of T_C on the mean rare earth ionic radius and later by DFT calculations [8] using the local spin density approximation (LSDA). In addition, it was found that a change in Pr-O distances could have induced a variation of Pr valence. The experimental measurements gave contradictory results regarding this aspect [9-13], but there were many clues about a migration of Pr ions in Ba sites (Pr_{Ba}). Many researchers produced single crystals or polycrystalline Pr123 with several synthesis techniques and found that superconductivity was disappearing for the samples with at least ~10% of Pr_{Ba} defects [14-20]. Subsequently DFT calculations confirmed these experimental results [21, 22]. The presence of Pr_{Ba} defects was demonstrated by the observation of oxygen in the anti-chain site (between the Cu(1) atoms of the two chains), which indicated a trivalent cation in a neighbouring Ba site [3]. This feature induced a variation of the stoichiometry of the Pr123 with the following reaction [23]:

$$PrBa_2Cu_3O_{6+\delta} \longrightarrow \frac{1}{1+\alpha} Pr_{1+\alpha}Ba_{2-\alpha}Cu_3O_{6+\delta} + \frac{3\alpha}{1+\alpha} BaCuO_2$$

It is well known that the production in air of the nominal stoichiometry 1:2:3 leads to the presence of an impurity phase of $BaCuO_2$, while the solid solution starts from the Pr-rich compounds $Pr_{1+x}Ba_{2-x}Cu_3O_{6+\delta}$ with x = 0.08 [24]. Under particular synthesis conditions (inert or pure O_2 atmosphere with calcination times longer than 2 days), some authors [14, 23, 25, 26] claimed to produce polycrystalline stoichiometric Pr123 without impurities, although Park et al. found impurity phases after 10 days of calcinations with subliquidus anneal in 1 bar of oxygen atmosphere [27].

The Pr123 phase crystallizes in an orthorhombic structure with space group *Pmmm* (n° 47), but it can also present a tetragonal *P4/mmm* space group (n° 123) for quenched samples [28, 29] with oxygen content lower than 6.6-6.7 [23, 30]. A representation of the crystal structures is reported in Fig. 1, with lattice data taken from literature [30, 31] and images drawn with Vesta 3 software [32]. In addition to space group and cell parameters, the only differences between these lattice models are the descriptions of oxygen positions. In particular the equatorial oxygens of Cu(1) chains of the orthorhombic structure are regularly disposed, while in the tetragonal they are randomly positioned. Statistically, half of the tetragonal cells will present Cu(1) chains oriented along *a* axis and half along *b* axis, always with square planar coordination geometry. This introduces a half occupied additional oxygen position in the Cu(1) chains of the structural model used to describe the tetragonal compounds.

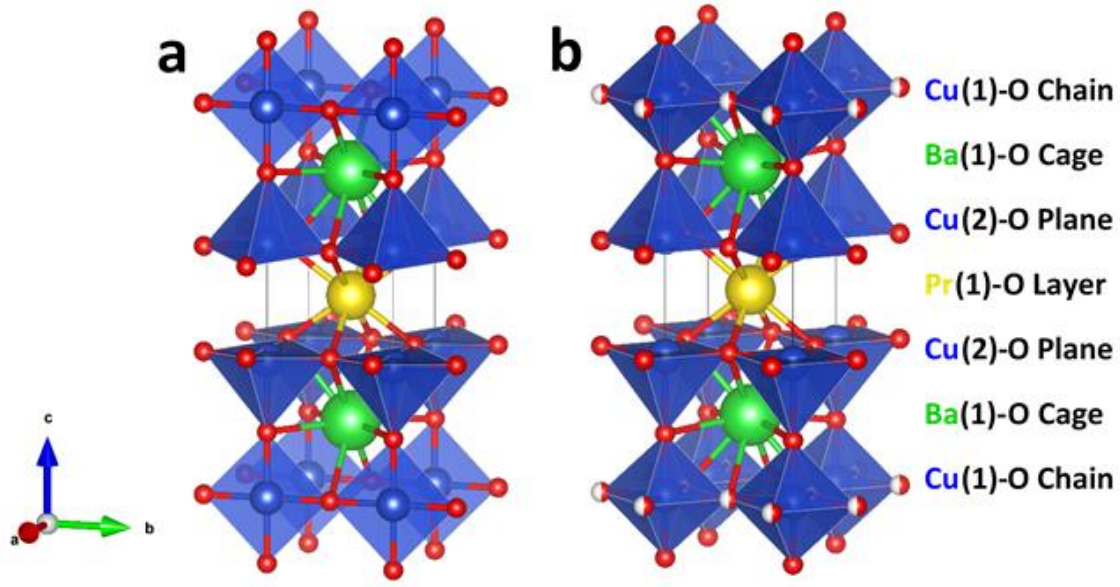

Figure 1: Representation of the orthorhombic (panel a) and tetragonal (panel b) crystal structures for $PrBa_2Cu_3O_7$ composition. Pr cations are represented in yellow, Ba in green, Cu in blue (inside the Cu-O polyhedra), O in red and vacancies in white.

Quenched samples annealed in oxygen showed a phase transition from tetragonal to orthorhombic [27], while samples annealed in inert atmosphere were reported to arrange in a tetragonal phase together with reduced oxygen content [23]. The orthorhombic-tetragonal phase transition was also observed in the Pr-rich series of materials $Pr_{1+x}Ba_{2-x}Cu_3O_{6+\delta}$ starting from x = 0.30 [24] or 0.20 [29, 33]. Kravchenko et al. [29] found out that the orthorhombic-tetragonal phase transition occurred at about 750 °C for the stoichiometric Pr123 phase. The increase of the cell parameter *c* was pointed out as one of the main parameters to discriminate the Pr123 with superconductivity (high *c* and low δ) from the not superconducting one. The main reason could be the presence of Pr ions in the Ba site (Pr_{Ba}), which also induced the formation of the secondary phase $BaCuO_2$ [6].

The peculiar structure of Pr123 generated interest and curiosity, due to high number of layered vacancies, located preferentially in Cu(1)-O(1) chains [23, 28,

31, 34], presence of copper in different oxidation states ($Cu^{+}/Cu^{2+}/Cu^{3+}$), divided in Cu(2) planes (Coordination N° = 5) and Cu(1) chains (C.N° = 4) [7, 31, 35, 36] and absence of cobalt [37-39]. In addition, barium-layered perovskites with praseodymium as rare earth usually showed superior performances as IT-SOFC cathodes compared to corresponding compounds with other rare earths [40-45]. Thus, $PrBa_2Cu_3O_7$ composition was selected as possible material suitable as SOFC cathode.

Concerning this 1:2:3 structure, investigations as SOFC cathodes were carried out only on compounds with Y as rare earth. In 1990, Steele and coworkers [46], first hypothesized the possible utilization of YBCO for oxygen related application, due to high oxygen flux and ionic conductivity results (10^{-2}-10^{-3} S/cm at 700 °C [46, 47]). However, the performance of pure YBCO were not promising in comparison with typical cathode materials used in those years, i.e., $La_{1-x}Sr_xTMO_3$ (*TM* = Transition metal) simple perovskites [48]. High polarization losses, attributed to phase degradation, were reported by Fletcher et al. [49], while the first record of impedance spectroscopy results indicated ASR values of 1.2 $\Omega \cdot cm^2$ on GDC ($Gd_{0.1}Ce_{0.9}O_{1.95}$) and 10 $\Omega \cdot cm^2$ on YSZ ($Y_{0.15}Zr_{0.85}O_{1.925}$) at 700 °C [50]. Krüger et al. [51] demonstrated that lattice parameters of “near-equilibrium” slow-cooled YBCO can depends even on the use of carbonate precursors, e.g. $BaCO_3$, which is found in traces (0.1-0.6 wt. %) at the grain boundaries of YBCO [52]. Subsequently, complete or partial cations substitutions were introduced to enhance the stability of the phase. Stability improvements were obtained replacing entirely barium with strontium [53]. The authors also claimed that the main instability problem was located at Cu(1)-O chains, thus they produced two compositions with Fe or Co doping the Cu site. Global conductivity measurements on $YSr_2Cu_2CoO_7$ showed values in the range of 15-35 S/cm between 500 and 700 °C, while values of 4-5 S/cm for $YSr_2Cu_2FeO_7$ in the same temperature range. In addition, chemical compatibility studies were carried out between these compounds and typical SOFC electrolytes, i.e., YSZ and GDC. The results revealed that with YSZ, the insulating $SrZrO_3$ was found as reactive phase, while test with GDC showed the presence of an impurity only above 1000 °C. The reactive phases obtained between $YSr_2Cu_2(Co,Fe)O_7$ and GDC were identified as a conductive fluorite compounds $(Y,Ce)_2Sr_2Cu_{3-x}(Co,Fe)_xO_{9+y}$. The authors claimed that these reactive phases show better conductivity values than the 1:2:3 structures, reducing the relevance of impurity presence. Although they proposed these compounds as SOFC cathode candidates, they did not publish any further electrochemical measurement. Few years later, Šimo et al. [54] tested the electrochemical performance of the $Y_{1-x}Sr_{2+x}Cu_{3-y}Co_yO_7$ materials. They found that single-phase samples with $y > 1$ were produced tailoring the Y/Sr ratio, and the introduction of extra Co improved the performances. Conductivities between 55 and 70 S/cm in the 500-700 °C range and an ASR equal to 0.08 $\Omega \cdot cm^2$ at 700 °C were measured for the sample $Y_{0.95}Sr_{0.05}Cu_{1.7}Co_{1.3}O_7$ screen-printed on GDC support pellet. Concerning Pr123 composition, no investigations as cathode material are available in literature, to the best of our knowledge. Aim of this work is the synthesis and characterization of the $PrBa_2Cu_3O_{6+\delta}$ compound as cathode for IT-SOFCs.

The main possible issue with the application of Pr123 as SOFC cathode is the possible low electronic conductivity, suggested by the literature [4, 16, 17, 33, 55-57]. The available resistivity data are reported in the 0 and 300 K range, typical of superconductive investigations, and show values between 10^{-2} and 1 $\Omega \cdot cm^2$ at 300 K. A very high fluctuation of the results is observed for materials produced under different synthesis conditions (Fig. 2). In addition, the cause of bad performance as SOFC cathodes of many layered cuprates is the low electronic conductivity [58-60]. As suggested by layered *RE*BaM_2O_x perovskites, a compositional tailoring is considered as a possible solution to improve conductivity. The substitution of Ba with Sr is a well-known strategy for perovskites and is reported to improve the global conductivity also for $PrBa_{2-x}Sr_xCu_3O_{6+\delta}$ series [55, 61]. The subsolidus phase relation of these compositions shows the existence of single-phase compounds in the range $0.2 \leq x \leq 0.6$ [62]. Thus, in addition to the basic Pr123 stoichiometry, a second composition with 25% of Ba substituted by Sr is also investigated.

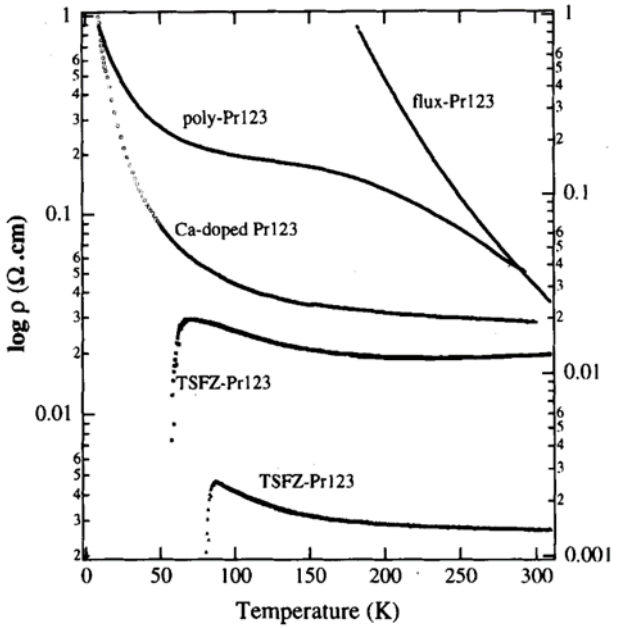

Figure 2: Resistivity values of $PrBa_2Cu_3O_{6+\delta}$ polycrystalline and single crystals grown by flux and Travelling-Solvent Floating-Zone (TSFZ) methods in the 0-300 K range. The results of polycrystalline $PrBa_{1.5}Ca_{0.5}Cu_3O_{6+\delta}$ are also reported [17].

2. Materials and Method

$PrBa_2Cu_3O_{6+\delta}$ (P) and $PrBa_{1.5}Sr_{0.5}Cu_3O_{6+\delta}$ (PS) were produced by molten citrate technique, to obtain homogeneous cations dispersion, typical of wet syntheses. The desired amount of Pr_6O_{11} (Solvay, 99.9%), $Ba(CO_3)_2$ (Sigma Aldrich, 99.5%), $Sr(CO_3)_2$ (Cerac, 99.5%) and CuO (Sigma Aldrich, 99.7%) were dissolved into the minimum amount of nitric acid (HNO_3, Honeywell, 65% diluted) and distilled water necessary to form a clear solution. Afterwards, citric acid monohydrated ($C_6H_8O_7 \cdot H_2O$, Sigma Aldrich, 99%) was added to the nitric solution in large excess to ensure enough amount of citric acid to disperse the precursors. The molar ratio of citric acid and metal ions was fixed at 7. More details can be found

in reference [63]. The solution was heated at 140 °C to obtain a viscous slurry and then calcined in oven at 360 °C for 12 hours. The obtained powders were grinded and calcined at 950 °C for 12 hours with a heating and cooling rate of 5 °C/min. After another grinding step and XRPD measurement, the calcination at 950 °C was performed again to ensure the complete crystallization and to reach the thermodynamic equilibrium of the solid solution. The resulting powders were grinded again and analysed with a PANalitycal X'pert PRO MPD diffractometer in Bragg-Brentano θ-θ geometry equipped with Cu-K_α radiation source and X'Celerator multi-strip detector. The diffraction patterns were collected within an angular range 8-80° 2θ with a step of 0.017° 2θ and counting time of 0.5 seconds. Sintered pellets of cathodic materials were prepared by die pressing and followed by sintering at 980 °C for 6 hours with heating and cooling ramps of 2 °C/min. The global conductivity was determined in air using a four-probe technique between 100 and 800 °C. The measurements were carried out both increasing and decreasing the temperature. The test started at 800 °C, measuring the conductivity while cooling (1 or 2 °C/min) until 100 °C. Then, the measurement continued while the sample was heated again up to 800 °C, followed by a second cooling test to ensure the reproducibility. Electrochemical impedance spectroscopy (EIS) tests were performed on symmetric button cells, consisting of porous electrode layers deposited on each side of dense electrolyte pellets. The pellets (~1.6 cm diameter) were produced by die pressing commercial gadolinium-doped ceria powders (GDC20: $Ce_{0.8}Gd_{0.2}O_{2-\delta}$, Marion Tech.), followed by sintering at 1500 °C for 6 hours. The relative density of the pellets was calculated by the ratio of geometrical density of the pellets and theoretical GDC density (~7.24 g/cm^3 [64, 65]). All the pellets showed a relative density higher than 95%, suitable as support for EIS measurements. A slurry of the cathode material (69 wt. % solid content) was prepared mixing the powders with terpineol (dispersant), isopropyl alcohol (solvent) and ethyl cellulose (binder), respectively 15 wt. %, 15 wt. % and 1 wt. %. The cathodic slurry was accurately mixed to obtain a homogeneous ink for screen printing. The ink was screen printed through a 0.9 cm diameter mask, on each side of GDC pellets, followed by calcination at 900 °C for 1 hour with 1 °C/min heating and cooling rates. After the first EIS tests, a thin praseodymium-doped ceria (PrDC: $Ce_{0.7}Pr_{0.3}O_{2-\delta}$, Praxair) interlayer was applied via screen printing on both sides of the GDC pellets before depositing the cathode, in order to avoid the formation of insulating phases at the cathode-electrolyte interface. The cathode inks were subsequently screen printed on top of PrDC interlayers. The PrDC ink was composed of 39 wt. % powders, 50 wt. % solvent, 10 wt. % dispersant and 1 wt. % binder. The PrDC interlayers were calcined at 1250 °C for 2 hours with rates of 1 °C/min. The measurements were carried out in the range 10^6-10^{-2} Hz using a Solartron Modulab XM model 2100A potentiostat, with *ac* amplitude of 50 mV. Gold grids were used as current collectors. Data were fitted using the equivalent circuit model (ECM) technique with Zview® software (Scribner Associates Inc.). More details of the setup used to perform impedance tests are provided in reference [66]. The morphological features of the interlayers and the porous electrodes of the symmetric cells were assessed also after the EIS tests via Scanning Electron Microscopy (SEM) using a Carl Zeiss EVO50VP instrument.

3. Results and Discussion

3.1. XRPD Characterization

The powders are analysed with XRPD technique to evaluate the formation of Pr123 and the presence of impurity phases. Fig. 3 reports the spectra of P and PS samples after the second calcination at 950 °C.

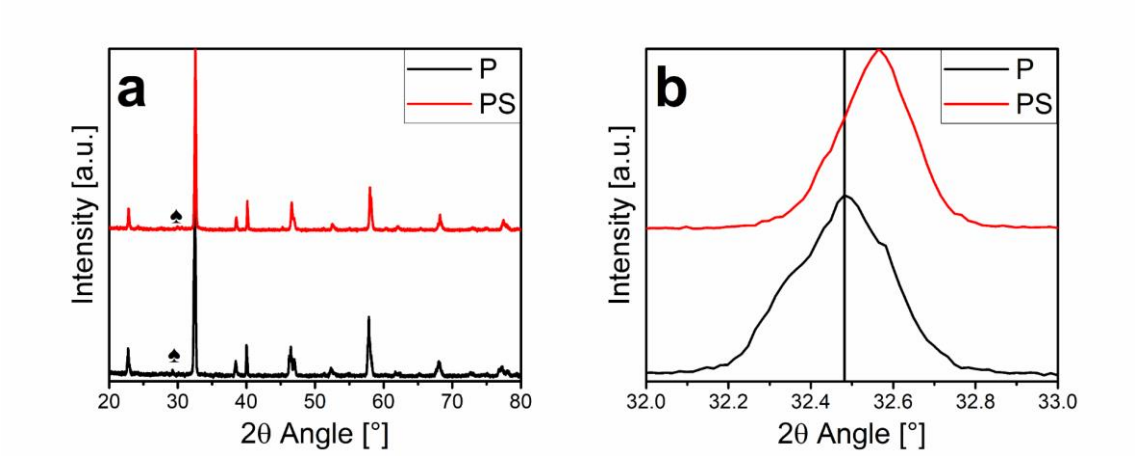

Figure 3: XRPD patterns for P and PS samples in the 20-80 °2θ range (panel a) and highlight of the main peak in the 32-33 °2θ range (panel b). Peaks of impurity phases are marked with ♠ for $BaCuO_2$.

The spectra show that the desired phase was successfully produced. Both compounds crystallize in an orthorhombic crystal lattice (space group *Pmmm*, n° 47) with slightly different lattice dimensions (COD ID 1520852 [30]). The introduction of Sr induces a slight shift of the peaks towards higher angles, which suggests a reduction of the cell parameters (COD ID 1533656 [62]). Small impurity peaks were found for both the composition at 29.2 and 29.9° 2θ and they were associated to $BaCuO_2$ (COD ID 1525807 [25]), as widely reported in literature for the Pr123 compound [23-25, 27, 30, 67, 68]. On the contrary, the presence of impurity phase in PS sample is not in agreement with Song et al. solid solution investigation [62].

3.2. Conductivity Measurements

The global electrical conductivity was measured in air with a four-probe technique during cooling and heating cycles. The results are reported in Fig. 4.

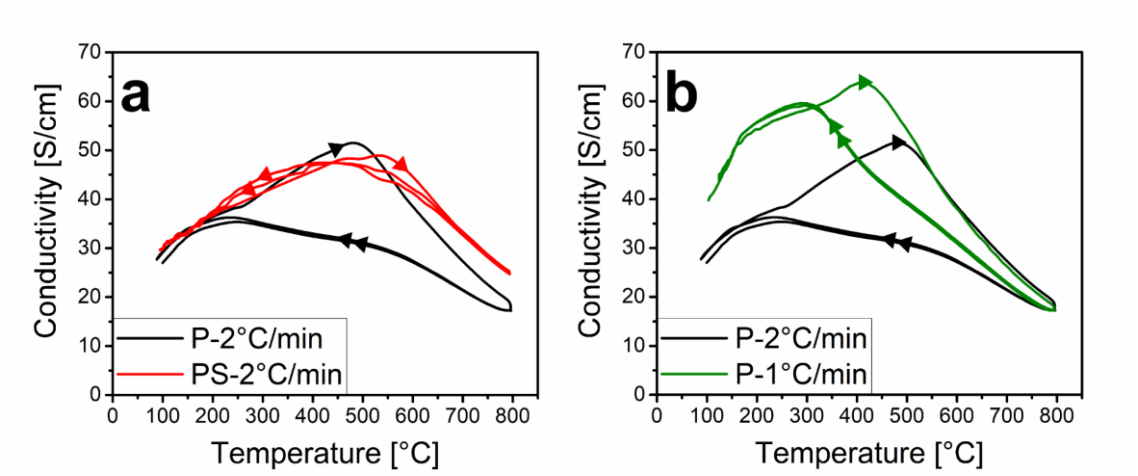

Figure 4: Electrical conductivity measurements on P and PS samples with heating and cooling rates of 2 °C/min (panel a). Comparison of conductivity measurements on P samples with different rates (panel b).

Panel a shows the results of the test performed on P and PS. The conductivity values vary between 20 and 60 S/cm in the operating temperature range of IT-SOFC. For both compounds, the conductivity increases with temperature up to 500-550 °C, while it decreases at higher temperatures. The temperature variation is expected to modify the oxygen content (6+δ) of the material, which changes the charge equilibrium of electron holes and charge carriers in the crystal structure. This equilibrium is the origin of the variation of conductivities, both electronic and ionic, with temperature. The performed tests measure the global conductivity, but electronic conductivity is typically several orders of magnitude higher than the ionic one [69-72].

The substitution of Ba with Sr does not remarkably increase the conductivity. The conductivity of PS is very similar to the values measured for P sample during the heating step. However, during the cooling ramps, a significant reduction of the conductivity of P is observed. The cooling is performed twice to ensure reproducibility. This generates a pronounced hysteresis, which is an indication of slow kinetics of oxygen equilibration inside the crystal structure. The rates of 2 °C/min were found to be too quick compared to the ability of P to exchange oxygen with the surrounding atmosphere during the test. Hence, an additional measurement was carried out with slower ramps. This second conductivity test was repeated to ensure the reliability of the results. Panel b reports the comparison of the results obtained with different rates. The green curve (P-1°C/min) starts from 800 °C at the same value of the black curve (P-2°C/min) but reaches higher values when the temperature is below 500 °C. At 300 °C, a steep reduction begins, but the conductivity at 100 °C is still higher than P-2°C/min. During the following reheating step, the hysteresis of P-1°C/min is reduced, but still present. The slower heating/cooling rates allow the material to exchange more oxygen and to approach the equilibrium. Above 500 °C, the two curves completely overlap until the temperature reduction. The second cooling steps reveal a complete reproducibility of both the measurements. The maximum of global electrical conductivity is found at about 420 °C during the slow heating step (64 S/cm). Overall, the conductivity is lower than the lower limit of 100 S/cm,

proposed by Steele [73] to ensure the absence of conduction limitations in the cathodic polarization resistance. For an electrode, this limitation leads to an increase of the ohmic resistance of the EIS measurement, due to the lack of electrons for the reaction in the cathodic sites. This issue will be discussed in more details in paragraph 3.3.

The results of conductivity for P are a clear indication of the occurrence of a slow process of equilibration of the structure, driven by temperature variations above 300 °C. The structure has insufficient time to reach the complete equilibrium with a 1 °C/min ramp. The change of oxidation states of the mixed valence cations influences the conductivity values due to the concentration of electron carriers (holes, h●). The valences of the equilibrium condition for the cations distribution is a function of the ions mobility induced by temperature variations. This is accompanied by a variation of the oxygen content in the crystal structure.

The work carried out by Sansom et al. [74] on cuprates with the 1:2:3 structure, $YSr_2Cu_2CoO_7$ and $YSr_2Cu_2FeO_7$, reports a hysteresis in conductivity values between measurements on reducing and oxidizing. The authors interpret this result as a poor oxide ion transport, poor oxygen surface exchange kinetics, or significant structural changes on varying oxygen partial pressure. For YBCO, different resistivity values during cooling and heating are measured even with ramps of 0.1 °C/min. A small hysteresis is observed around the orthorhombic-tetragonal phase transition temperature [75]. Furukawa et al. [76] proposed a model where the slow equilibration of the oxygen in the structure was driven by a 'moving boundary' oxidation mechanism [77]. Before reaching the equilibrium after a temperature variation, the particles of YBCO are composed of both tetragonal and orthorhombic phases. The transition occurs in correlation with an increase of copper valence, hence with the oxygen content of the structure coming from the air. Since the tetragonal phase is stable at high temperature, when the temperature is reduced, an oxidation of the structure occurs. This oxidation begins from the outer shell of the tetragonal YBCO grains, producing an orthorhombic-tetragonal interface that slowly moves towards the centre of the particle. Once the orthorhombic phase is all over the surface of the particle, the molecular oxygen requires a two-step process to further oxidize the inner tetragonal phase [77, 78]. This is probably the same process occurring during heating and cooling Pr123 sintered samples for conductivity measurements. The hysteresis observed is an effect of the kinetic rates of both oxygen surface and bulk diffusion of the orthorhombic outer shell in Pr123 grains.

3.3. Electrochemical Impedance Spectroscopy (EIS)

The production of the first symmetrical P/GDC/P cell reveals a reactivity issue between the electrolyte and the electrode. The P layers are deposited via screen printing, using a circular mask with a diameter of 9 mm, on both sides of a 16 mm GDC pellet. After the calcination at 900 °C, the GDC pellet appears darker in the surroundings of the cathode layer. This effect is related to an ion migration and reaction between P and GDC. After the EIS measurement, the cathode layer is bleached away with a droplet of nitric acid and subsequently, the pellet is placed on a rotating support and analysed with XRD (Fig. 5a). Panel a shows the

diffraction pattern of the *post mortem* cell after removal of the cathode layer. A very small peak at ~32° 2θ is still visible and is associated to the main peak of P. The other reflections are related to GDC, but also additional peaks are present at 41.0, 50.8, 59.4 and 67.2° 2θ. This undesired phase is identified as $BaCeO_3$ (COD ID 1521059 [79]), a simple perovskite widely studied as proton conductor [80]. The main peak of this phase is located at 28.6° 2θ, but this angle coincides with GDC and PrDC main peak positions. $BaCeO_3$ oxide presents a very low global conductivity, but mixed electronic and ionic conduction appears when doped with trivalent cations [81, 82].

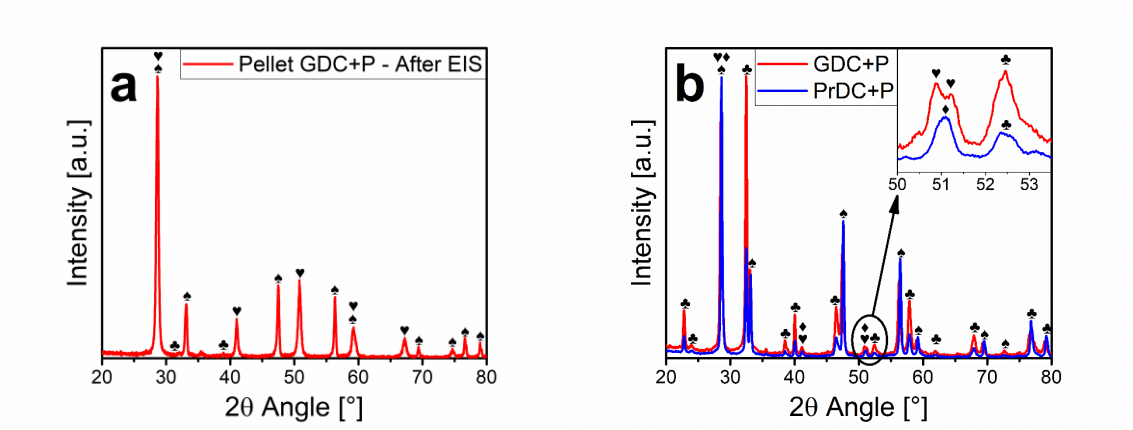

Figure 5: XRD pattern of GDC pellet of the cell used for EIS test, after bleaching the P layer (panel a). Panel b reports XRPD patterns of 50-50 wt. % P-(Gd or Pr)DC mixtures after calcination at 900 °C for 3 hours. The inset shows a magnification of 50-53.5° 2θ range. Peaks of GDC and PrDC are marked with ♠, peaks of P with ♣, while the remaining peaks belong to impurity phases (♥ for $BaCeO_3$ and ♦ for $BaPrO_3$).

Due to the formation of undesired phases, the introduction of a buffer layer to prevent the formation of $BaCeO_3$ was fundamental to evaluate the real cathodic activity of these compounds. PrDC ($Ce_{0.7}Pr_{0.3}O_{2-\delta}$) was selected as a possible candidate as buffer material for the interlayer, since it represents a compromise between the cubic structure of GDC (*Fm-3m*, space group #225) and the same rare earth of Pr123, which reduces the Pr gradient at the interface. Furthermore, the work of Flura et al. [83] shows positive EIS results on testing cells with PrDC as interlayer. PrDC is a MIEC compound due to the presence of the additional redox couple Pr^{3+}-Pr^{4+}, contrarily to the GDC, which only conducts O^{2-} ions [84-87]. Reactivity tests are carried out on powders of P with GDC and PrDC. First, a 50:50 wt. % mixture of P and PrDC is grinded and calcined at 900 °C for 3 hours, then XRPD is performed on the resulting powders. The XRPD patterns (Fig. 5b) show the peaks of GDC or PrDC (♠) and P (♣) together with weak reflections belonging to impurity phases, at the same angles of $BaCeO_3$. However, as it is possible to notice from the inset of Fig. 5b, the reflections at 50-52° 2θ reveal a clear variation in the impurity phase for the GDC+P and the PrDC+P mixtures. A similar peak splitting is observed in literature on the Ba*RE*$O_{3\pm\delta}$ series [88, 89]. A possible explanation is that Pr ions partially or completely substitute Ce in $BaCeO_3$. Moreover, $BaCeO_3$ and $BaPrO_3$ have the same crystal structure (*Pbnm*, space group #62), with slightly different cell

parameters [79], which explains the differences in the peaks at 50-52° 2θ. In addition, the solid solution $BaCe_{1-x}Pr_xO_3$ is single phase for any degree of substitution, x, and increasing Pr content gradually reduces the lattice parameters [81, 82]. As a matter of fact, the identification of the exact composition of the impurity phases is very difficult, in particular due to the relatively small amounts in the powder mixtures. However, an undesired reaction of P occurs with both GDC and PrDC above 900 °C, but the results of EIS tests reveal the differences related to the presence of PrDC interlayer. The partial or complete substitution of Ce with Pr strongly influences the polarization resistances, due to the increase of electronic conductivity of the reactive phase at the interface cathode-electrolyte.

In Fig. 6, the EIS results are reported for P samples at 582 °C (panel a) and 781 °C (panel b) for the cell configuration with and without PrDC interlayer. The results for the PS compound are reported at 600 °C (panel c) and 800 °C (panel d). In order to ensure the reliability of the data, EIS tests were continuously performed until the consecutive acquirement of two identical spectra. With the interlayer, an evident reduction of the resistance is observed in every condition for both the compounds. At 800 °C, the presence of the PrDC interlayer reduces the ASR of 3-4 times, while at lower temperature the improvement due to PrDC reaches even a 30-fold reduction. These considerable improvements are attributed to an enhancement of the transfer of charges at the interface cathode-electrolyte, although the few microns thick interlayer is present. Theoretically, the introduction of an interlayer produces an additional interface, which is reflected into a new contribution in EIS spectra [83]. However, the EIS results show that the resistive contribution of PrDC interlayer is negligible compared to the contributed related to the reactive interface accidentally produced by heating at high temperature P or PS in direct contact with GDC. Therefore, it is important to verify that PrDC interlayer can be considered a part of the electrolyte support and does not play a role in any ORR kinetic step. In order to ensure that the only effect of PrDC interlayers is to prevent the formation of the insulating phase at the cathode-electrolyte interface, an EIS test on PrDC as cathode material is carried out. A symmetrical cell is prepared but, instead of applying cathodic inks, a platinum paste is directly screen printed on the PrDC layer. The Pt layer works as current collector to compensate the relatively low PrDC electronic conduction (total conductivity ~10^{-2} S/cm at 700 °C [85, 87]) compared to cathode requirements.

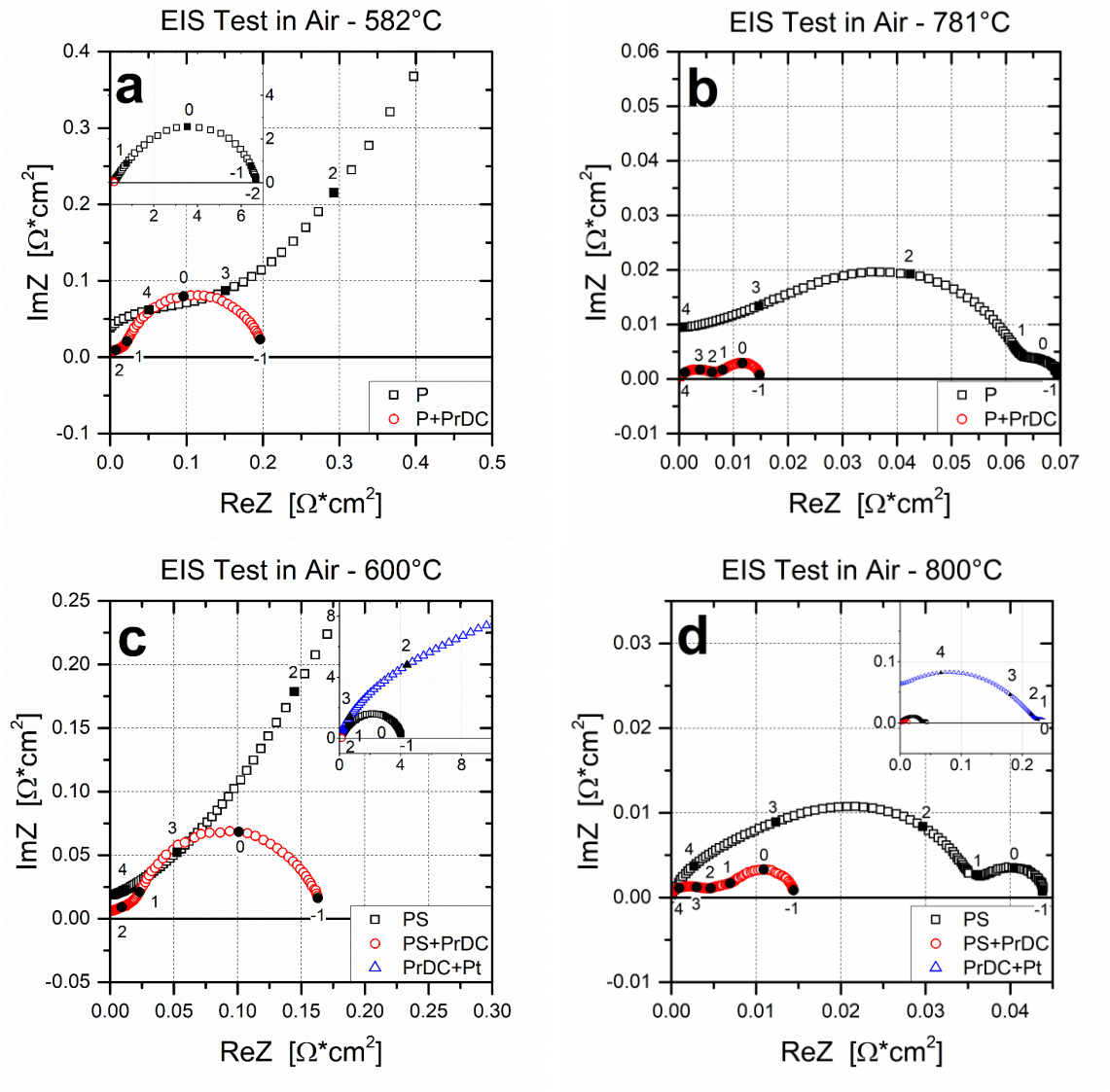

Figure 6: Normalized Nyquist plots of P (panels a-b) and PS samples (panels c-d) at low and high temperature, in the 10 kHz-0.1 Hz frequency range (10 kHz-0.01 Hz for inset in panel a). Empty symbols are experimental data and numbers near filled symbols represent the logarithm of the frequency decade. Black squares □ are the results of tests with (P or PS)/GDC/(P or PS) symmetrical configuration. Red circles ○ are the results of tests with (P or PS)/PrDC/GDC/PrDC/(P or PS) symmetrical configuration. Blue triangles Δ are the results of tests with Pt/PrDC/GDC/PrDC/Pt symmetrical configuration.

The EIS results are reported in Fig. 6 at 600 °C (panel c) and 800 °C (panel d). The resistances are an order of magnitude higher than the values of P+PrDC at high temperature, while at low temperature the tests produce open arcs without a low frequency intercept. These shapes are typical of measurements carried out on electrolyte materials [90, 91]. Therefore, these results suggest that PrDC is not suitable as cathode material [92], but works particularly well as interlayer [83] to avoid the formation of insulating $BaCeO_3$ impurity. In addition, an EIS test with Pt current collector directly applied on a GDC dense pellet is also carried out to verify that the polarization resistances are representative purely of ORR kinetic processes, without effects of poor current extraction or delamination of the layers.

The ohmic resistances of the EIS results are normalized with geometrical parameters to obtain the ionic conductivity of GDC supports. These values are used as references for the conductivity calculated from EIS tests on P and PS cells. The results are reported in the Arrhenius plot of Fig. 7 and show very good agreement between the different tests, indicating an excellent contact of the layers. Table 1 summarizes the apparent activation energy (E_{ACT}) of GDC ionic conductivity, calculated from the slopes in the Arrhenius plot of (Fig. 7). The E_{ACT} values range from 0.68 to 0.76 eV. These values are in agreement with both the results of GDC conductivity measured with Pt and literature data [93-103]. In addition, E_{ACT} of ASR curves are also reported in Table 1, divided in high (HT: 850-700 °C) and low temperature (LT: 650-450 °C) ranges for tests with PrDC interlayer.

Table 1: Summary of apparent activation energies (E_{ACT}) of GDC conductivity and ASR values obtained from EIS tests on P and PS samples, with and without PrDC interlayer. E_{ACT} values of ASR for samples with interlayer are divided in high temperature (HT: 850-700 °C) and low temperature (LT: 650-450 °C) ranges.

	$PrBa_2Cu_3O_{6+\delta}$		**$PrBa_{1.5}Sr_{0.5}Cu_3O_{6+\delta}$**	
Cell Configuration	**P**	**P+PrDC**	**PS**	**PS+PrDC**
E_{ACT} (GDC Cond)	0.68 eV	0.74 eV	0.72 eV	0.76 eV
E_{ACT} (ASR) - HT	1.75 eV	0.39 eV	1.87 eV	0.37 eV
E_{ACT} (ASR) - LT		1.86 eV		1.82 eV

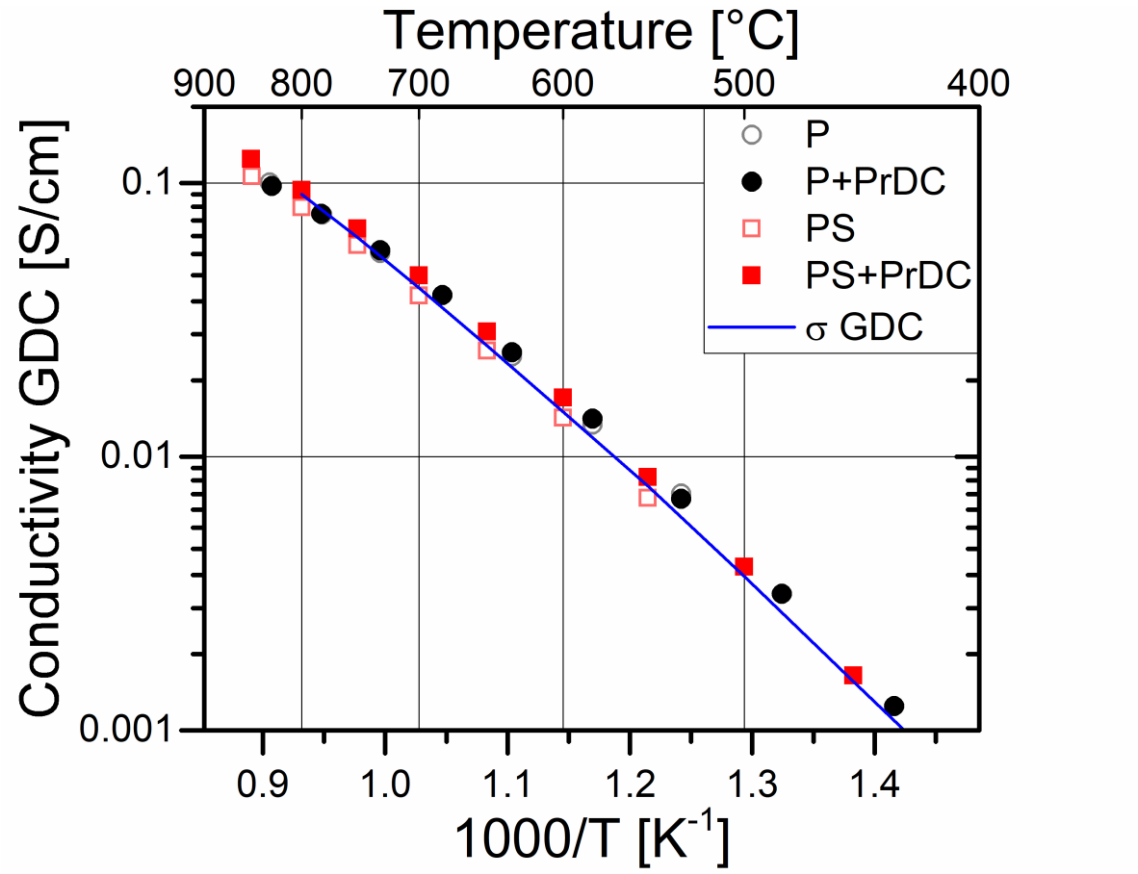

Figure 7: Arrhenius plot of the conductivity of GDC pellets used for EIS measurements for P and PS samples with (full symbols) and without PrDC interlayer (empty symbols). The line is the result of the direct measurement of a GDC20 pellet with Pt current collector.

Fig. 8 shows the Arrhenius plot of the ASR curves: the improvement due to the presence of PrDC is remarkable. The results of the samples with PrDC are very encouraging, since, already at 600 °C, they almost hit the target values of 0.15 $\Omega \cdot cm^2$ proposed by Steele [73] for the consideration as promising cathode material. The curves of the samples without PrDC are linear, while the curves of the samples with PrDC bend at high temperature. This is an indication of a change of the rate determining step (RDS) at different temperatures. Kolchina et al. [104 793] also find similar non-linear ASR curves in Arrhenius plot for $Pr_{2-x}Ce_xCuO_4$ compounds, but with smaller E_{ACT} values and smaller differences in the slopes, compared to our results. Hart et al. report a variation in E_{ACT} at 700 °C for graded cathodes $La_{0.85}Sr_{0.15}MnO_3$-YSZ, but with higher values (1.42-1.51 eV) in the HT range compared to LT range (1.01-1.05 eV) [105].

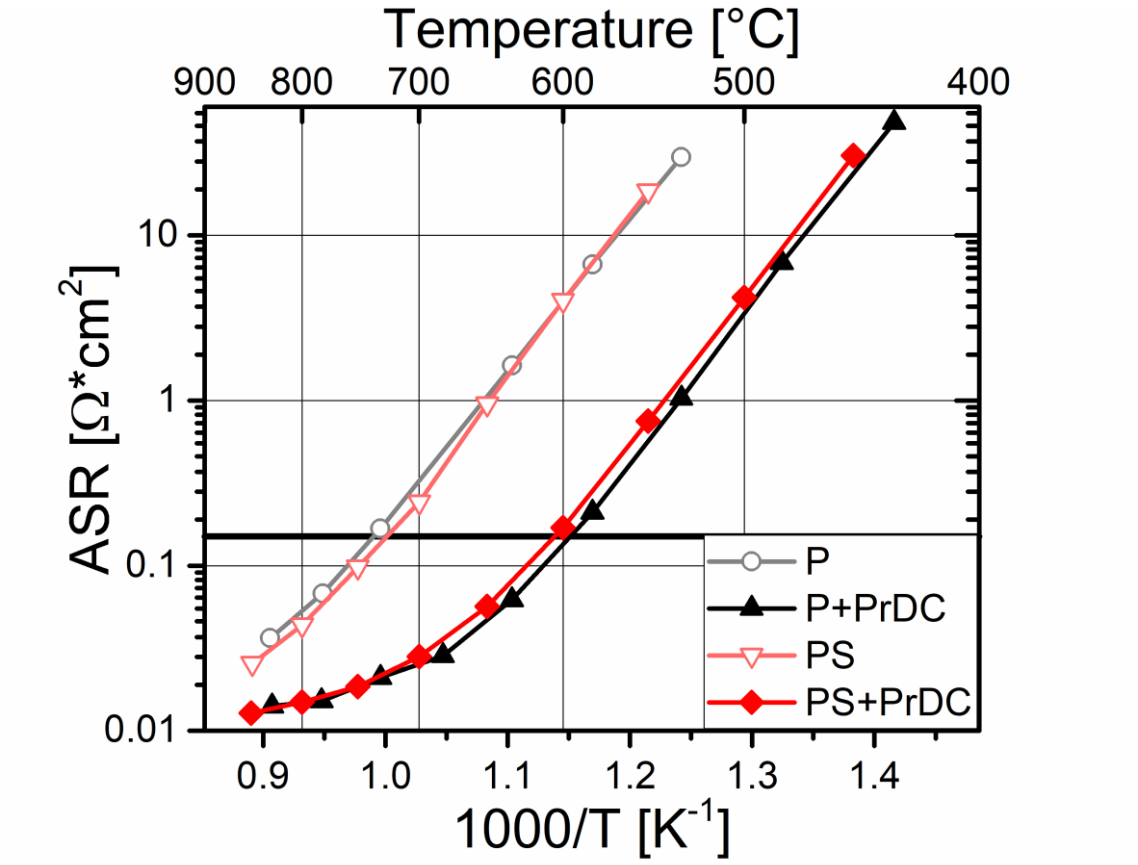

Figure 8: Arrhenius plot of ASR values for P and PS samples with (full symbols) and without PrDC interlayer (empty symbols).

Another evidence of a variation in the kinetic mechanisms of the ORR is the change of the shapes of the arcs related to the introduction of the PrDC interlayer (Fig. 6). The cell configuration influences the process kinetics. A possible additional indication of this effect lies in that, upon introducing the PrDC interlayer, a large resistance contribution is removed, and the spectra consist of arcs, which are smaller and differently shaped than those obtained without the interlayer. These aspects reveal a complex kinetic mechanism.

The apparent E_{ACT} for samples without PrDC are equal to 1.75 and 1.87 eV for P and PS, respectively. These values are similar to those of the P+PrDC (1.86 eV) and PS+PrDC (1.82 eV) samples in the LT range, suggesting the possibility of the same RDS of the process. These apparent E_{ACT} values are quite large compared to typical literature values, although some compounds present similarities. Regarding the cathodes with 1:2:3 structure, Ralph et al. [50] find for activation energies of 1.9 eV for YBCO on GDC10 supports, and of 2.0 eV on YSZ. Arrhenius plots of ASR values are not reported and an eventual slope variation cannot be observed. On the contrary, for $Y_{1-x}Sr_{2+x}Cu_{3-y}Co_yO_7$ compounds, a drastic increase of ASR is reported reducing the temperature from 700 to 650 °C [54]. The authors claimed that is related to electrochemical decomposition, but do not explain why it occurs only in this temperature range. Typical E_{ACT} for Co-based layered perovskites range between 0.91 eV and 1.86 eV [106], with the highest values found by Kim et al. [107] for $GdBaCo_{2-x}Fe_xO_{5+\delta}$

(1.20-1.86 eV) and $GdBaCo_{2-x}Fe_xO_{5+\delta}$ (1.45-1.80 eV). Similar activation energies are reported for the $La_{2-x}Sr_xCoTiO_6$ (1.58-1.64 eV) series of composite cathodes (mixture 1:1 w:w with YSZ) [108]. Some simple perovskites containing Sr also show relatively high apparent E_{ACT}, e.g., 1.54 eV for $Pr_{0.3}Sr_{0.7}CoO_{3-\delta}$ [109], 1.65 eV for $Sr_{0.7}Y_{0.3}CoO_{3-\delta}$ [110] and 2.03 eV for $Sm_{0.5}Sr_{0.5}MnO_3$ [111]. In addition, other peculiar oxide structures present comparable values: 1.63 eV for $YBaCu_4O_{7+\delta}$ [112] and 1.65 eV for $La_4BaCu_3Co_3O_{13+\delta}$ [113]. Very low E_{ACT} values are instead obtained in the HT range, i.e., 0.37-0.39 eV. Such values indicate that the reason for this slope change is the overlapping of different resistances, among which, at high temperature, result predominant a contribution generated by non-electrochemical phenomena. A physical process that can generate an arc in Nyquist plot with almost negligible temperature dependence (E_{ACT} ~0) is gas diffusion [114]. The arc associated with gas diffusion limitation is located at low frequencies (f < 10 Hz) in EIS spectra with low resistances, typically at high temperature. In Fig. 6b and Fig. 6d a convoluted arc at high frequencies is observed, which gives rise to about 0.01 $\Omega \cdot cm^2$ resistance. This contribution is predominant for samples with PrDC, resulting in almost two third of the total ASR. Additionally, above 700 °C the ASR curves tend to a horizontal asymptote (Fig. 8). All these features suggest that gas diffusion limitations become the limiting step at high temperatures. In order to verify the association of this phenomenon with the LF arc and its relevance in terms of resistance, an analysis with ECM method is carried out.

3.4. Equivalent Circuit Model (ECM)

The equivalent circuit model is applied to separate different contributions simultaneously present in the spectra. Each process step is simulated with a resistance in parallel with a capacitive element (CPE) that results in a depressed semi-circle in Nyquist plot. Once the model is selected, the parameters of the circuital elements are obtained by fitting to the experimental points. The fitted parameters appear linear in logarithmic scale if they belong to the same elementary process step. Thus, the goodness of the deconvolution is evaluated by the linearity of the curves. Trial-and-error fittings are performed to obtain results satisfactory enough to be considered reliable indications of the processes occurring for these samples during the ORR.

The first hypothesis required by ECM technique is the selection of an equivalent circuit suitable to fit the EIS spectra. From the shape of the arcs, it is evident that more than a circuit is necessary, because the higher the temperature, the flatter the EIS spectra becomes. This is related to the fact that the arcs associated to the contributions with the highest E_{ACT} cover the other arcs with negligible resistances at low temperatures. Hence, models with a smaller number of elements are employed for fittings at low temperature. The fittings are performed starting from the highest temperature experiments, testing a model with a resistance (R Ohm) in series with several R//CPE parallel elements. The initial value of these R//CPE contributions is suggested by the shape of the arcs and further corroborated by data analysis. When the temperature is reduced, it is necessary to remove one or two R//CPE elements to avoid inconsistent results.

In the selection of the models, the lowest number of elements that allows an accurate fitting a spectrum is preferred, in order to avoid mathematical agreements without chemical meaning.

The parameters of each element allow to calculate relaxation frequencies (f_{REL}) and double layer capacitances (C_{eq}), as follows:

$$f_{rel_i} = \frac{1}{(2\pi \cdot R_i \cdot Q_i)^{\frac{1}{n_i}}}$$

$$C_{eq_i} = R_i^{\left(\frac{1-n_i}{n_i}\right)} \cdot Q_i^{\frac{1}{n_i}}$$

R_i are the values of the resistive elements, Q_i the capacitances of the CPE_i element, and n_i are the exponential of CPE_i elements. f_{rel} is an indication of the characteristic frequency, where the centre of the arc is located, and is the inverse of the characteristic time of the process step. C is the double layer capacitance of the geometrical interface involved in the reaction step and is related to the microstructure, e.g., roughness, tortuosity, vacancies, grain boundaries [115, 116]. The logarithm of f_{REL} and C_{eq} are plotted as a function of the inverse of the temperature. Fig. 9 shows the results of P samples with (full symbols) and without PrDC (empty symbols), together with corresponding fittings (solid and dashed lines). Similar results are obtained for PS samples. The linearity of the curves is an indication of the reliability of the ECM results. The equivalent circuit model with 3R//CPE elements, employed to fit the experimental spectra are reported in Fig. 9.

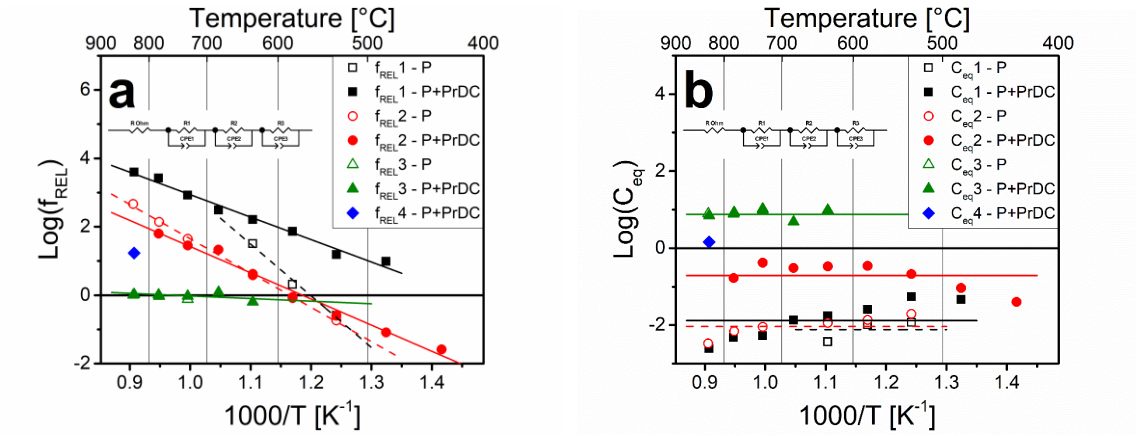

Figure 9: Logarithmic plots of relaxation frequencies (panel a) and equivalent capacitances (panel b) as a function of the inverse of temperature of the single contributions separated through ECM deconvolution. The results are reported for P samples with (full symbols) and without PrDC interlayer (empty symbols). Lines are the fitting results of P (dashed) and P+PrDC (solid) values.

Two elements are required to fit the spectra of the samples without interlayer. Instead, the P+PrDC sample requires 3 elements in the fitting above 600 °C. The elements necessary to fit P spectra are 2; though, below 650 °C, f_{REL} and C_{eq} values drastically change, indicating a change of the associated process. Above this temperature a low frequency process is obtained ($f_{REL}3$), while below the results of the deconvolution indicate a high frequency reaction step ($f_{REL}1$). This

HF process is introduced in the model because the arcs start showing a Gerischer-like shape at high frequencies (inset in Fig. 6a) and an additional R//CPE with n_{CPE} = 0.5-0.6 is required. A linear high frequency branch is not observed in the spectra collected on PS, whose arcs are almost perfect semicircles. On the contrary, for P+PrDC a HF contribution ($f_{REL}1$ and $C_{eq}1$) occurs in a higher frequency range and is present at all the temperatures. Another contribution is present in both the samples with and without interlayer with frequencies in a middle frequency range. Anomalous outcomes of f_{REL} and C_{eq} are obtained for the MF contribution of P+PrDC at the 831 °C, which is considered an outlier associated to a different contribution ($f_{REL}4$ and $C_{eq}4$). Beside this exception, very satisfactory fittings are obtained, and similar results are found for PS samples. Overall, the ECM results correctly show that relaxation frequencies increase with temperature because the reaction steps speed up, while the capacitances are almost constant because attributed to morphological parameters.

The polarization resistance contributions are reported in Arrhenius plots in Fig. 10 for P and PS samples with (panels a and c respectively) and without PrDC interlayer (panels b and d). For each process, the E_{ACT} gives an indication of the associated reaction step. A clear evidence is obtained for the LF process: an absence of temperature dependency is typical of gas diffusion process, which is an almost non-activated phenomenon. The high capacitance values are also supporting this hypothesis [117-120]. With respect to the PS sample, at 750 °C the second contribution has a R_{POL} which can be reasonably associated to gas diffusion limitations, but f_{REL} is 4 orders of magnitude higher than the results of measurements at 800 and 850 °C. C_{eq} is also 3 orders of magnitude lower than correspondent contributions at higher temperatures. Hence this contribution at 750 °C is considered as a HF process similar to those found in other deconvolutions and named R1 (black empty square in Fig. 10c), while at 800 °C and 850 °C it is associated to gas diffusion in LF range (R3, green empty triangles).

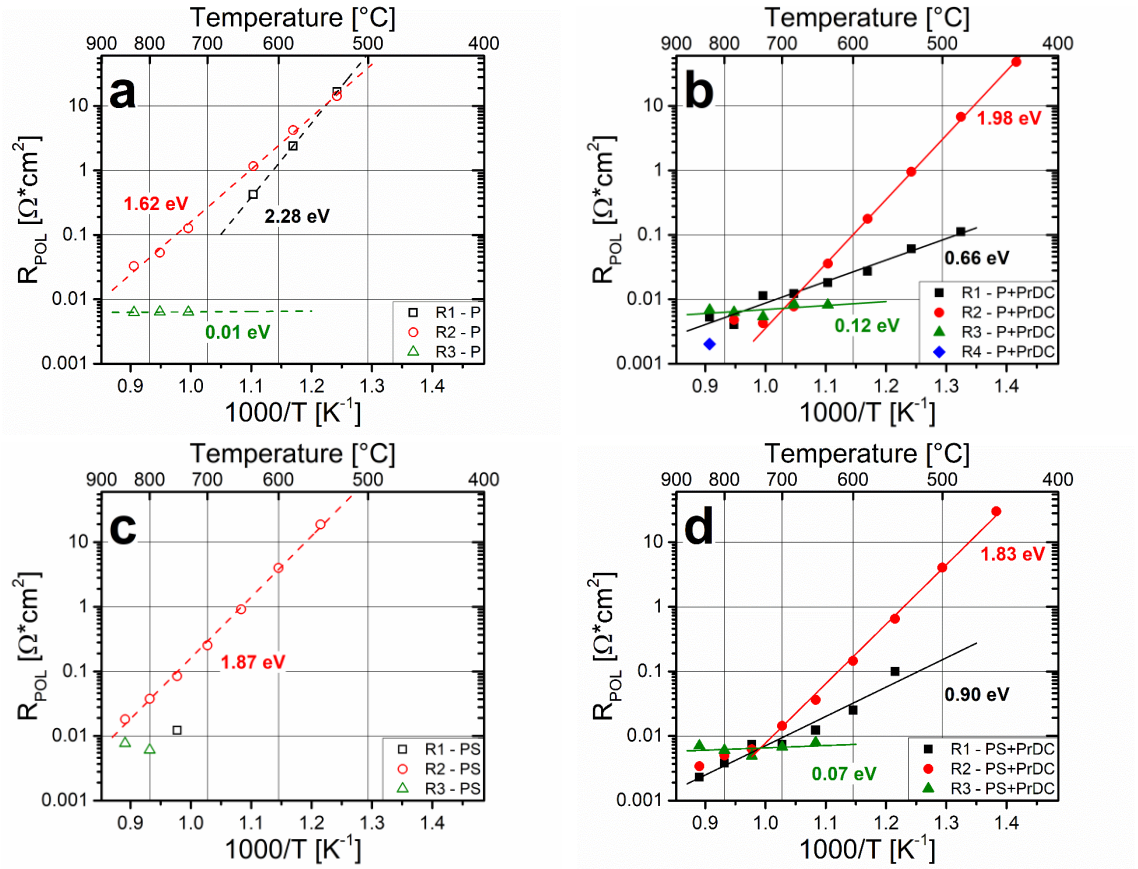

Figure 10: Logarithmic plots of polarization resistance as a function of the inverse of temperature of the single contributions separated through ECM deconvolution. The results are reported for P (panels a and b) and PS (panels c and d) samples with (full symbols) and without PrDC interlayer (empty symbols). Lines are the fitting results of P (dashed) and P+PrDC (solid) values.

Considering the R3 as the contribution associated with gas diffusion limitations, it is clear that for samples with the interlayer, this phenomenon becomes prevalent upon increasing the temperature, due to higher E_{ACT} of the other contributions. For this reason, the resistances R1 and R2 tend to disappear, in particular for PS+PrDC (Fig. 10d). Above 700 °C, the R1 and R2 of samples with interlayer are outliers, quite distant from the predictions of the fitting lines, indicating that some modifications took place. In particular, the last point presents R_{POL}, f_{REL} and C_{eq} values incompatible with the other points of the process. This suggests the possibility of a fourth process step involved, with frequencies between the LF and MF contributions and a not negligible resistance value. Even the HF resistance becomes more and more relevant increasing the temperature.

The association of MF and HF contributions to a reaction step is not possible, since E_{ACT} values alone are not sufficient to corroborate any assumption. However, based on literature results, it is possible to speculate that the HF process is related to a charge transfer across an interface, e.g., grain boundaries or cathode-electrolyte interface. These processes involving ionic species usually occur at very high frequencies (10^2-10^4 Hz) [119, 121, 122].

The modifications during the measurements can have different origins, since this symmetrical cell system is complex. Several structural and morphological transformations can take place during the EIS tests at high temperature. First, a reactivity issue is identified and evaluated through XRD analysis (Fig. 5). The resistances of cathode-interlayer-electrolyte interfaces can evolve at high temperature if the undesired reaction is ongoing during the EIS tests. Furthermore, a phase transition from orthorhombic to tetragonal lattice takes place above 700-750 °C [29]. During EIS tests above this temperature range, the crystal lattices of P and PS materials are shifting towards a more symmetrical structure. Theoretically, this change in space group is connected to a reduction of the oxygen content, 6+δ, of the material [23], hence a higher number of oxygen vacancies. These aspects can induce changes in R_{POL} slope and C_{eq} values of ion transfer processes, independently of the interface involved. These results suggest that the optimal application temperature of Pr123 is up to 650 °C.

The results of P reveal an indisputable stability issue of the symmetrical cells for EIS testing. At the beginning of the project, this issue was interpreted as a reactivity between the materials of cell components in contact at high temperature. The interlayer introduction mitigates the problem related to large resistivity values, but the presence of another phase complicates the sample structures. In particular, a slight but constant shift of EIS spectra is sometimes observed between measurements repetition at the same temperature. In order to ensure the reliability of the data, EIS tests were continuously performed until the consecutive acquirement of two identical spectra. The collection of several measurements increased the time required to test a cell, but also allowed the evaluation of the reasons of these shifts. A rigid shift of the EIS results between two measurements means that the ohmic resistance of the cell is changing. R_{Ohm} is related to the resistance of the electrolyte pellet, cables and interconnections. The pellet is the component that mostly contributes to R_{Ohm} for electrolyte-supported cells, but if the conductivity falls below a threshold level, resistive contributions can arise. The indicative value of the requirement of electronic conductivity for the electrode is considered 100 S/cm, but also the presence of some issues can hamper electron transfer, e.g., an insulating layer at the interface, a detachment of the electrode, bad contacting between elements, and so on. Thus, the explanation for the shift can be represented by the slow formation of an insulating phase between P and PrDC. However, the reason of some peculiar results was unclear, and some questions arisen. During several tests, the instability shift reduced the R_{Ohm} between two measurements. In particular, the instability below 700 °C aroused curiosity because much longer waits than usual were necessary to stabilize the results. Before starting the first EIS test at 850 °C, the cells were calcined at 900 °C (±1 °C/min rate) for 1 hour and spent a night (~15-20 hours) in temperature to stabilize completely. Then, no sign of instability was recorded among the 3 tests performed at 800 and 750 °C. Hence, the reactivity issue between 700 and 600 °C cannot be the only reason of the instability, since the production of an insulating phase at the interface electrolyte/interlayer/electrode is reasonably a temperature-activated process. The higher the temperature, the stronger interface modifications occur, both if their origin is reactivity or microstructural densification of the contact surface. On the contrary, the variation of R_{Ohm} below 700 °C can be associated to a

modification of the Pr123 structure, due to the T-O phase transition occurring at this temperature, as previously anticipated. A possible explanation is the coexistence of the two Pr123 structures in a single phase or in a single grain. A situation similar to Y123, with a ‘moving boundary’ oxidation mechanism, can explain the very long stabilization time at intermediate temperatures [76], [77]. In addition, this hypothesis could explain the asymmetrical peak broadening and the valley flatness observed in XRPD spectra (Fig. 3) and conductivity hysteresis (Fig. 4).

Fig. 11 reports SEM images of the symmetrical cell after the EIS measurements of P sample, at 100x, 1kx, 5kx and 15kx magnification (respectively panels a, b, c and d). The thickness of the electrolyte dense pellet is 1.1 mm, while the porous P layer and PrDC interlayer are respectively equal to ~32 and 2.5 µm. The cathode microstructure is not optimized and the grain size is higher than the typical value of 0.5 µm, suggested for cathode powders. This is probably related to the beginning of the sintering process observed already after the first thermal treatment at 950 °C. After the calcinations, the compounds inside the crucibles appear as a single block of material. A grinding step is performed, but the crystal growth exceeded and the grain size cannot be easily reduced.

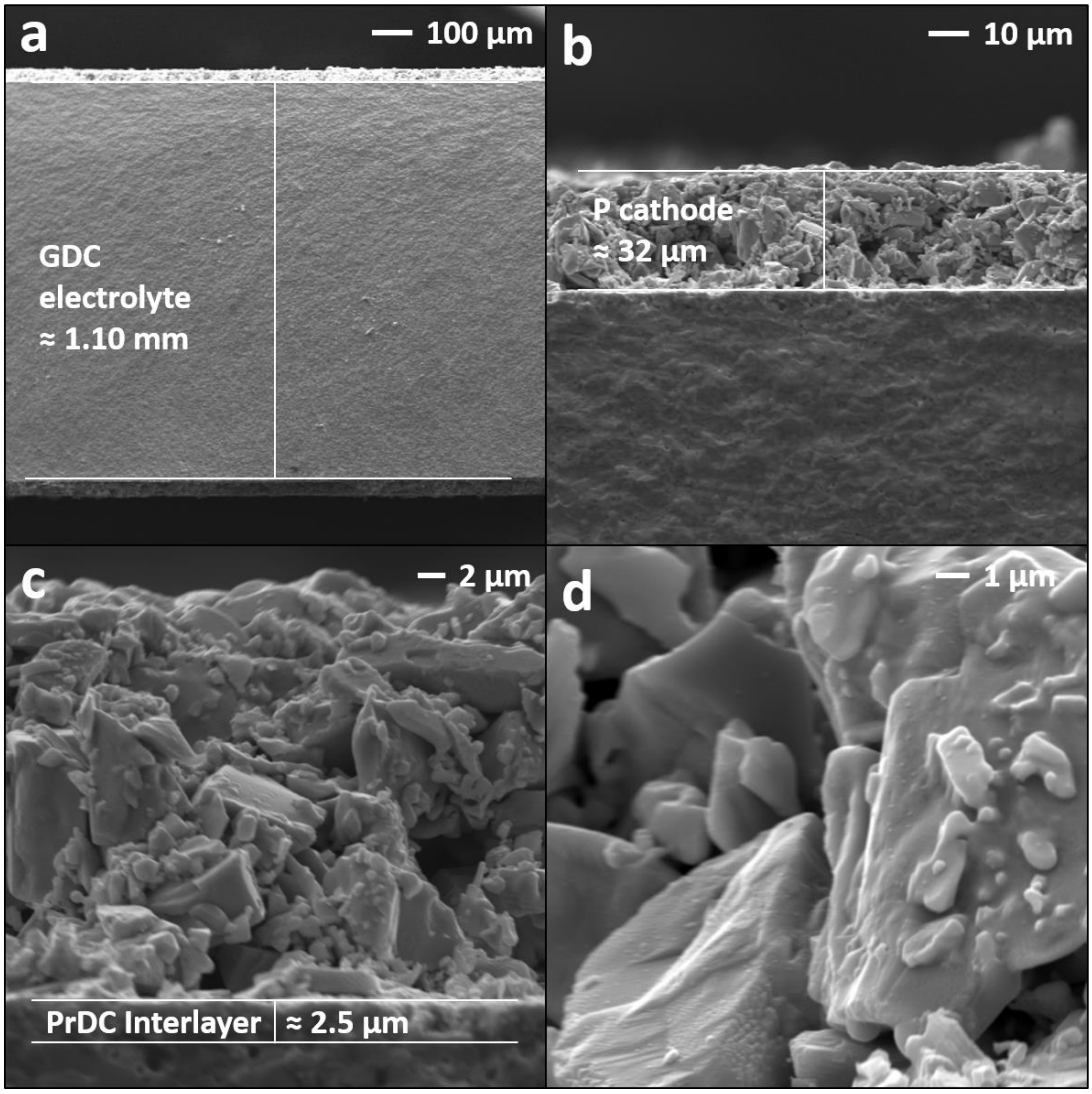

Figure 11: Secondary electrons SEM images of the symmetrical cell used for EIS measurements of P sample, at 100x, 1kx, 5kx and 15kx magnification, respectively panels a, b, c and d.

As it is possible to see from Fig. 11c, P powders present a bimodal distribution of particles diameters, with modes of about 1 and 10 µm. Laser granulometry measurements performed on the powders used for screen printing inks confirmed the SEM results. A bimodal particles size distribution is obtained after 5 minutes of ultrasounds. The two modes are located at 0.8 and 13.2 µm, while the median (i.e., d_{50}) is at 6.3 µm. furthermore, SEM images reveal a peculiar grain surface with submicron particles sintered on the surface of bigger particles and superficial roughness on other particles (Fig. 11d).

4. Conclusions

$PrBa_2Cu_3O_{6+\delta}$ (P) and $PrBa_{1.5}Sr_{0.5}Cu_3O_{6+\delta}$ (PS) compounds are evaluated as cathodes for IT-SOFCs. The P and PS samples crystallize in an orthorhombic lattice with slightly smaller cell parameters for PS. The conductivity

measurements reveal a hysteresis in the heating and cooling ramps, which suggests either slow oxygen surface transfer or a bulk oxygen interdiffusion. The conductivities range from 20 to 60 S/cm in the IT-SOFC operating temperature range, but no electronic conduction limitations are observed during EIS tests. The reactivity between GDC and P produces an insulating phase identified as $BaCeO_3$. The introduction of a PrDC interlayer results in a partial or complete substitution of Ce with Pr in $BaCeO_3$, which improves ion transfers at the cathode-electrolyte interface. The electrochemical tests show negligible differences between the resistances measured for samples P and PS. On the contrary, the presence of PrDC interlayer reduces the ASR of an order of magnitude below 750 °C. The improvement due to the interlayer is less significant at high temperature because the ASR curves of P+PrDC and PS+PrDC present a change in the activation energy. Anyhow, the electrochemical performance is very promising and the goal of 0.15 $\Omega \cdot cm^2$ is almost fulfilled even at 600 °C (ASR of PS+PrDC: 0.17 $\Omega \cdot cm^2$). The equivalent circuit analysis shows that three main resistive processes are involved in the ORR. The LF process is identified as gas diffusion and its limitations become negligible below 650 °C. Above 700 °C, several parameters influence the EIS results and further investigations are necessary to separate these aspects and improve the performance of these compounds. The results of ECM suggest that the optimal application temperature of Pr123 is up to 650 °C, due to possible structural or morphological modifications occurring at higher temperature.

References

[1] J.G. Bednorz and K.A. Müller, *Zeitschrift für Physik B Condensed Matter*, **64, 2** (1986) 189-193. DOI: 10.1007/BF01303701

[2] M.K. Wu, J.R. Ashburn, C.J. Torng, P.H. Hor, R.L. Meng, L. Gao, Z.J. Huang, Y.Q. Wang and C.W. Chu, *Phys. Rev. Lett.*, **58, 9** (1987) 908-910.

[3] H.A. Blackstead, D.B. Chrisey, J.D. Dow, J.S. Horwitz, A.E. Klunzinger and D.B. Pulling, *Phys. Lett. A*, **207, 1** (1995) 109-112. DOI: https://doi.org/10.1016/0375-9601(95)00653-K

[4] Z. Zou, K. Oka, T. Ito and Y. Nishihara, *Japanese Journal of Applied Physics*, **36, 1A** (1997) L18.

[5] J.D. Dow and D.R. Harshman, *Int. J. Mod Phys B*, **21, 18-19** (2007) 3086-3095.

[6] H.A. Blackstead and J.D. Dow, *Solid State Commun.*, **115, 3** (2000) 137-140. DOI: https://doi.org/10.1016/S0038-1098(00)00141-1

[7] R. Fehrenbacher and T.M. Rice, *Phys. Rev. Lett.*, **70, 22** (1993) 3471-3474. DOI: 10.1103/PhysRevLett.70.3471

[8] A.I. Liechtenstein and I.I. Mazin, *Phys. Rev. Lett.*, **74, 6** (1995) 1000-1003. DOI: 10.1103/PhysRevLett.74.1000

[9] S. Horn, J. Cai, S.A. Shaheen, Y. Jeon, M. Croft, C.L. Chang and M.L. denBoer, *Phys. Rev. B*, **36, 7** (1987) 3895-3898. DOI: 10.1103/PhysRevB.36.3895

[10] J.S. Kang, J.W. Allen, Z.X. Shen, W.P. Ellis, J.J. Yeh, B.W. Lee, M.B. Maple, W.E. Spicer and I. Lindau, *Journal of the Less Common Metals*, **148, 1** (1989) 121-132. DOI: https://doi.org/10.1016/0022-5088(89)90018-0
[11] F.W. Lytle, G. van der Laan, R.B. Greegor, E.M. Larson, C.E. Violet and J. Wong, *Phys. Rev. B*, **41, 13** (1990) 8955-8963. DOI: 10.1103/PhysRevB.41.8955
[12] C.H. Booth, F. Bridges, J.B. Boyce, T. Claeson, Z.X. Zhao and P. Cervantes, *Phys. Rev. B*, **49, 5** (1994) 3432-3442. DOI: 10.1103/PhysRevB.49.3432
[13] M. Khaled, N.L. Saini, K.B. Garg and F. Studer, *Solid State Commun.*, **100, 11** (1996) 773-776. DOI: https://doi.org/10.1016/S0038-1098(96)00513-3
[14] C. Stari, L. Cichetto, C.H.M.A. Peres, V.A.G. Rivera, S. Sergeenkov, C.A. Cardoso, E. Marega and F.M. Araújo-Moreira, *J. Alloys Compd.*, **528,** (2012) 135-140. DOI: 10.1016/j.jallcom.2012.03.048
[15] M. Calamiotou, A. Gantis, I. Margiolaki, D. Palles, E. Siranidi and E. Liarokapis, *J. Phys.: Condens. Matter*, **20, 39** (2008). DOI: 10.1088/0953-8984/20/39/395224
[16] Z. Zou, J. Ye, K. Oka and Y. Nishihara, *Phys. Rev. Lett.*, **80, 5** (1998) 1074-1077.
[17] Y. Nishihara, Z. Zou, J. Ye, K. Oka, T. Minawa, H. Kawanaka and H. Bando, *Bull. Mater. Sci.*, **22, 3** (1999) 257-263. DOI: 10.1007/BF02749929
[18] A. Shukla, B. Barbiellini, A. Erb, A. Manuel, T. Buslaps, V. Honkimäki and P. Suortti, *Phys. Rev. B*, **59, 18** (1999) 12127-12131.
[19] F.M. Araujo-Moreira, P.N. Lisboa-Filho, S.M. Zanetti, E.R. Leite and W.A. Ortiz, *Physica B: Condensed Matter*, **284-288,** (2000) 1033-1034. DOI: https://doi.org/10.1016/S0921-4526(99)02374-1
[20] H.A. Blackstead, J.D. Dow, I. Felner and W.B. Yelon, *Phys. Rev. B*, **63, 9** (2001) 094517.
[21] V. Ghanbarian and M.R. Mohammadizadeh, *The European Physical Journal B*, **61, 3** (2008) 309-318. DOI: 10.1140/epjb/e2008-00080-6
[22] A. Tavana, M. Shirazi and M. Akhavan, *physica status solidi (b)*, **246, 10** (2009) 2287-2293. DOI: 10.1002/pssb.200945033
[23] M.E. López-Morales, D. Ríos-Jara, J. Tagüea, R. Escudero, S. La Placa, A. Bezinge, V.Y. Lee, E.M. Engler and P.M. Grant, *Phys. Rev. B*, **41, 10** (1990) 6655-6667. DOI: 10.1103/PhysRevB.41.6655
[24] G.B. Song, J.K. Liang, F.S. Liu, L.T. Yang, J. Luo and G.H. Rao, *Powder Diffr.*, **19, 4** (2004). DOI: 10.1154/1.1814981
[25] P.N. Lisboa-Filho, S.M. Zanetti, A.W. Mombrú, P.A.P. Nascente, E.R. Leite, W.A. Ortiz and F.M. Araújo-Moreira, *Supercond. Sci. Technol.*, **14, 8** (2001) 522.
[26] F.M. Araujo-Moreira, P.N. Lisboa-Filho, A.J.C. Lanfredi, W.A. Ortiz, S.M. Zanetti, E.R. Leite, A.W. Mombrú, L. Ghivelder, Y.G. Zhao and V. Venkatesan, *J. Magn. Magn. Mater.*, **226-230,** (2001) 283-284. DOI: https://doi.org/10.1016/S0304-8853(00)00801-5
[27] M. Park, M.J. Kramer, K.W. Dennis and R.W. McCallum, *Physica C: Superconductivity and its Applications*, **259, 1** (1996) 43-53. DOI: https://doi.org/10.1016/0921-4534(96)00006-8

[28] C.K. Lowe-Ma and T.A. Vanderah, *Physica C: Superconductivity*, **201, 3** (1992) 233-248. DOI: https://doi.org/10.1016/0921-4534(92)90469-S
[29] A.V. Kravchenko, E.A. Gudilin, I.V. Arkhangel'skii and Y.D. Tret'yakov, *Doklady Chemistry*, **385, 4** (2002) 199-202. DOI: 10.1023/A:1019993118104
[30] C. Bertrand, P. Galez, R.E. Gladyshevskii and J.L. Jorda, *Physica C: Superconductivity*, **321, 3** (1999) 151-161. DOI: https://doi.org/10.1016/S0921-4534(99)00369-X
[31] U. Amador, E. Morán, M.A. Alario-Franco, J. Ibáñez, J. Martín and T.S. Rey, *Solid State Ionics*, **63-65,** (1993) 858-865. DOI: https://doi.org/10.1016/0167-2738(93)90207-J
[32] K. Momma and F. Izumi, *J. Appl. Crystallogr.*, **44, 6** (2011) 1272-1276. DOI: doi:10.1107/S0021889811038970
[33] W.H. Tang and J. Gao, *Physica C: Superconductivity*, **315, 1** (1999) 66-70. DOI: https://doi.org/10.1016/S0921-4534(99)00192-6
[34] E. Morán, U. Amador, M. Barahona, M.A. Alario-Franco, A. Vegas and J. Rodríguez-Carvajal, *Solid State Commun.*, **67, 4** (1988) 369-372. DOI: https://doi.org/10.1016/0038-1098(88)91047-2
[35] J. Ye, Z. Zou, K. Oka, Y. Nishihara and T. Matsumoto, *J. Alloys Compd.*, **288, 1** (1999) 319-325. DOI: https://doi.org/10.1016/S0925-8388(99)00106-1
[36] T. Mizokawa, A. Ino, T. Yoshida, A. Fujimori, C. Kim, H. Eisaki, Z.-X. Shen, S. Horii, T. Kakeshita, S. Uchida, K. Tomimoto, S. Tajima and Y. Yamada, *Int. J. Mod Phys B*, **14, 29n31** (2000) 3602-3609. DOI: 10.1142/s021797920000412x
[37] N.A. Baharuddin, A. Muchtar and M.R. Somalu, *Int. J. Hydrogen Energy*, **42, 14** (2017) 9149-9155. DOI: 10.1016/j.ijhydene.2016.04.097
[38] F.S. da Silva and T.M. de Souza, *Int. J. Hydrogen Energy*, **42, 41** (2017) 26020-26036. DOI: 10.1016/j.ijhydene.2017.08.105
[39] Y. Zhang, R. Knibbe, J. Sunarso, Y. Zhong, W. Zhou, Z. Shao and Z. Zhu, *Adv Mater*, **29, 48** (2017). DOI: 10.1002/adma.201700132
[40] E. Chavez, M. Mueller, L. Mogni and A. Caneiro, *Journal of Physics: Conference Series*, **167,** (2009) 012043. DOI: 10.1088/1742-6596/167/1/012043
[41] X. Che, Y. Shen, H. Li and T. He, *J. Power Sources*, **222,** (2013) 288-293. DOI: 10.1016/j.jpowsour.2012.08.044
[42] F. Jin, H. Xu, W. Long, Y. Shen and T. He, *J. Power Sources*, **243,** (2013) 10-18. DOI: 10.1016/j.jpowsour.2013.05.187
[43] J.H. Kim, M. Cassidy, J.T.S. Irvine and J. Bae, *J. Electrochem. Soc.*, **156, 6** (2009) B682. DOI: 10.1149/1.3110989
[44] C. Rossignol, J.M. Ralph, J. Bae and J.T. Vaughey, *Solid State Ionics*, **175, 1-4** (2004) 59-61. DOI: 10.1016/j.ssi.2004.09.021
[45] H. Zhao, Y. Zheng, C. Yang, Y. Shen, Z. Du and K. Świerczek, *Int. J. Hydrogen Energy*, **38, 36** (2013) 16365-16372. DOI: 10.1016/j.ijhydene.2013.10.003
[46] D.J. Vischjager, A.A. van Zomeren, J. Schoonman, I. Kontoulis and B.C.H. Steele, *Solid State Ionics*, **40-41,** (1990) 810-814. DOI: https://doi.org/10.1016/0167-2738(90)90127-D
[47] J.L. MacManus, D.J. Fray and J.E. Evetts, *Physica C: Superconductivity*, **190, 4** (1992) 511-521. DOI: https://doi.org/10.1016/0921-4534(92)90713-M

[48] J. Fleig, *Annu. Rev. Mater. Res.*, **33, 1** (2003) 361-382. DOI: 10.1146/annurev.matsci.33.022802.093258
[49] J.G. Fletcher, J.T.S. Irvine, A.R. West, J.A. Labrincha, J.R. Frade and F.M.B. Marques, *Mater. Res. Bull.*, **29, 11** (1994) 1175-1182. DOI: https://doi.org/10.1016/0025-5408(94)90187-2
[50] J.M. Ralph, A.C. Schoeler and M. Krumpelt, *Journal of Materials Science*, **36, 5** (2001) 1161-1172. DOI: 10.1023/a:1004881825710
[51] C. Krüger, K. Conder, H. Schwer and E. Kaldis, *J. Solid State Chem.*, **134, 2** (1997) 356-361. DOI: https://doi.org/10.1006/jssc.1997.7579
[52] M. Maciejewski, A. Baiker, K. Conder, C. Krüger, J. Karpinski and E. Kaldis, *Physica C: Superconductivity*, **227, 3** (1994) 343-350. DOI: https://doi.org/10.1016/0921-4534(94)90091-4
[53] J.E.H. Sansom, H.A. Rudge-Pickard, G. Smith, P.R. Slater and M.S. Islam, *Solid State Ionics*, **175, 1** (2004) 99-102. DOI: https://doi.org/10.1016/j.ssi.2004.09.035
[54] F. Šimo, J.L. Payne, A. Demont, R. Sayers, M. Li, C.M. Collins, M.J. Pitcher, J.B. Claridge and M.J. Rosseinsky, *Solid State Sciences*, **37,** (2014) 23-32. DOI: 10.1016/j.solidstatesciences.2014.07.013
[55] Y.G. Zhao, Y.P. Li, B. Zhang, S.Y. Xiong, B. Yin, J.W. Li, S.Q. Guo, J.W. Xiong, D.J. Dong, B.S. Cao and B.L. Gu, *Physica C: Superconductivity*, **282-287, Part 2** (1997) 777-778. DOI: https://doi.org/10.1016/S0921-4534(97)00408-5
[56] H. Khosroabadi, M. Modarreszadeh, P. Taheri and M. Akhavan, *Journal of Superconductivity*, **17, 6** (2004) 749-753. DOI: 10.1007/s10948-004-0834-4
[57] H. Kawanaka, A. Saitoh, H. Bando and Y. Nishihara, *J. Alloys Compd.*, **408-412,** (2006) 1187-1189. DOI: https://doi.org/10.1016/j.jallcom.2004.12.123
[58] E. Boehm, J.M. Bassat, M.C. Steil, P. Dordor, F. Mauvy and J.C. Grenier, *Solid State Sciences*, **5, 7** (2003) 973-981. DOI: 10.1016/s1293-2558(03)00091-8
[59] Y.N. Kim and A. Manthiram, *J. Electrochem. Soc.*, **158, 3** (2011) B276. DOI: 10.1149/1.3527006
[60] T.A. Zhuravleva, *Russ. J. Electrochem.*, **47, 6** (2011) 676-680. DOI: 10.1134/s1023193511060164
[61] T. Sonobe and K. Yoshida, *Physica C: Superconductivity and its Applications*, **419, 3-4** (2005) 121-128. DOI: 10.1016/j.physc.2004.12.010
[62] G.B. Song, J.K. Liang, L.T. Yang, Q.L. Liu, G.Y. Liu, H.F. Yang and G.H. Rao, *J. Alloys Compd.*, **370, 1-2** (2004) 302-306. DOI: 10.1016/j.jallcom.2003.09.119
[63] G. Cordaro, A. Donazzi, R. Pelosato, C. Cristiani, G. Dotelli and I. Natali Sora, *ECS Transactions*, **78, 1** (2017) 507-520. DOI: 10.1149/07801.0507ecst
[64] I. Riess, D. Braunshtein and D.S. Tannhauser, *J. Am. Ceram. Soc.*, **64, 8** (1981) 479-485. DOI: doi:10.1111/j.1151-2916.1981.tb09901.x
[65] M.A.F. Öksüzömer, G. Dönmez, V. Sariboğa and T.G. Altinçekiç, *Ceram. Int.*, **39, 7** (2013) 7305-7315. DOI: https://doi.org/10.1016/j.ceramint.2013.02.069
[66] A. Flura, C. Nicollet, S. Fourcade, V. Vibhu, A. Rougier, J.M. Bassat and J.C. Grenier, *Electrochim. Acta*, **174,** (2015) 1030-1040. DOI: 10.1016/j.electacta.2015.06.084

[67] G. Collin, P.A. Albouy, P. Monod and M. Ribault, *Journal de Physique*, **51, 11** (1990) 1163-1177. DOI: 10.1051/jphys:0199000510110116300
[68] H.B. Radousky, *J. Mater. Res.*, **7, 7** (1992) 1917-1955. DOI: 10.1557/JMR.1992.1917
[69] C. Sun, R. Hui and J. Roller, *J. Solid State Electrochem.*, **14, 7** (2009) 1125-1144. DOI: 10.1007/s10008-009-0932-0
[70] S. Carter, A. Selcuk, R.J. Chater, J. Kajda, J.A. Kilner and B.C.H. Steele, *Solid State Ionics*, **53-56,** (1992) 597-605.
[71] A.A. Taskin, A.N. Lavrov and Y. Ando, *Prog. Solid State Chem.*, **35, 2-4** (2007) 481-490. DOI: 10.1016/j.progsolidstchem.2007.01.014
[72] A.V. Nikonov, K.A. Kuterbekov, K.Z. Bekmyrza and N.B. Pavzderin, *Eurasian Journal of Physics and Functional Materials*, **2, 3** (2018) 274-292. DOI: 10.29317/ejpfm.2018020309
[73] B.C.H. Steele, *Solid State Ionics*, **134,** (2000) 3-20.
[74] J.E.H. Sansom, E. Kendrick, H.A. Rudge-Pickard, M.S. Islam, A.J. Wright and P.R. Slater, *J. Mater. Chem.*, **15, 23** (2005) 2321-2327. DOI: 10.1039/B502641E
[75] P.P. Freitas and T.S. Plaskett, *Phys. Rev. B*, **36, 10** (1987) 5723-5726. DOI: 10.1103/PhysRevB.36.5723
[76] T. Furukawa, T. Shigematsu and N. Nakanishi, *Physica C: Superconductivity*, **204, 1** (1992) 103-108. DOI: https://doi.org/10.1016/0921-4534(92)90578-Z
[77] K. Conder, *Materials Science and Engineering: R: Reports*, **32, 2** (2001) 41-102. DOI: https://doi.org/10.1016/S0927-796X(00)00030-9
[78] M.D. Vazquez-Navarro, A thermogravimetric study of oxygen diffusion in YBa2Cu3O7-d, University of Cambridge, 1998.
[79] A.J. Jacobson, B.C. Tofield and B.E.F. Fender, *Acta Crystallographica Section B*, **28, 3** (1972) 956-961. DOI: doi:10.1107/S0567740872003462
[80] D. Medvedev, A. Murashkina, E. Pikalova, A. Demin, A. Podias and P. Tsiakaras, *Prog. Mater Sci.*, **60,** (2014) 72-129. DOI: 10.1016/j.pmatsci.2013.08.001
[81] J.F. Basbus, M. Moreno, A. Caneiro and L.V. Mogni, *J. Electrochem. Soc.*, **161, 10** (2014) F969-F976. DOI: 10.1149/2.0181410jes
[82] J.F. Basbus, A. Caneiro, L. Suescun, D.G. Lamas and L.V. Mogni, *Acta Crystallogr B Struct Sci Cryst Eng Mater*, **71, Pt 4** (2015) 455-462. DOI: 10.1107/S2052520615010203
[83] A. Flura, C. Nicollet, V. Vibhu, A. Rougier, J.-M. Bassat and J.-C. Grenier, *Electrochim. Acta*, **231,** (2017) 103-114. DOI: 10.1016/j.electacta.2017.02.019
[84] M. Nauer, C. Ftikos and B.C.H. Steele, *J. Eur. Ceram. Soc.*, **14, 6** (1994) 493-499. DOI: https://doi.org/10.1016/0955-2219(94)90118-X
[85] P. Shuk and M. Greenblatt, *Solid State Ionics*, **116, 3** (1999) 217-223. DOI: https://doi.org/10.1016/S0167-2738(98)00345-2
[86] T.S. Stefanik and H.L. Tuller, *MRS Proceedings*, **756,** (2002) EE10.18. DOI: 10.1557/PROC-756-EE10.8
[87] D.P. Fagg, I.P. Marozau, A.L. Shaula, V.V. Kharton and J.R. Frade, *J. Solid State Chem.*, **179, 11** (2006) 3347-3356. DOI: https://doi.org/10.1016/j.jssc.2006.06.028

[88] H. Horiuchi, T. Shishido, A. Saitow, M. Tanaka and S. Hosoya, *Materials Science and Engineering: A*, **312, 1** (2001) 237-243. DOI: https://doi.org/10.1016/S0921-5093(00)01893-1
[89] P.N. Lisboa-Filho, J.P. Rodrigues and W.A. Ortiz, *J. Mater. Sci. Lett.*, **22, 8** (2003) 623-627. DOI: 10.1023/a:1023362832455
[90] J. Patakangas, Y. Ma, Y. Jing and P. Lund, *J. Power Sources*, **263,** (2014) 315-331. DOI: 10.1016/j.jpowsour.2014.04.008
[91] N. Jaiswal, K. Tanwar, R. Suman, D. Kumar, S. Upadhyay and O. Parkash, *J. Alloys Compd.*, **781,** (2019) 984-1005. DOI: 10.1016/j.jallcom.2018.12.015
[92] R. Chockalingam, A.K. Ganguli and S. Basu, *J. Power Sources*, **250,** (2014) 80-89. DOI: 10.1016/j.jpowsour.2013.10.105
[93] V. Dusastre and J.A. Kilner, *Solid State Ionics*, **126,** (1999) 163-174.
[94] S. Kim and J. Maier, *J. Electrochem. Soc.*, **149, 10** (2002) J73-J83. DOI: 10.1149/1.1507597
[95] J. Faber, C. Geoffroy, A. Roux, A. Sylvestre and P. Abélard, *Appl. Phys. A*, **49, 3** (1989) 225-232. DOI: 10.1007/bf00616848
[96] S.A. Acharya, V.M. Gaikwad, V. Sathe and S.K. Kulkarni, *Appl. Phys. Lett.*, **104, 11** (2014). DOI: 10.1063/1.4869116
[97] M.G. Chourashiya, S.R. Bharadwaj and L.D. Jadhav, *Thin Solid Films*, **519, 2** (2010) 650-657. DOI: 10.1016/j.tsf.2010.08.110
[98] S.L. Reis, E.C.C. Souza and E.N.S. Muccillo, *Solid State Ionics*, **192, 1** (2011) 172-175. DOI: 10.1016/j.ssi.2010.06.017
[99] H. Duncan and A. Lasia, *Solid State Ionics*, **176, 15** (2005) 1429-1437. DOI: https://doi.org/10.1016/j.ssi.2005.03.018
[100] D. Pérez-Coll, P. Núñez, J.C. Ruiz-Morales, J. Peña-Martínez and J.R. Frade, *Electrochim. Acta*, **52, 5** (2007) 2001-2008. DOI: https://doi.org/10.1016/j.electacta.2006.08.009
[101] A. Jasper, J.A. Kilner and D.W. McComb, *Solid State Ionics*, **179, 21** (2008) 904-908. DOI: https://doi.org/10.1016/j.ssi.2008.02.001
[102] S. Dikmen, H. Aslanbay, E. Dikmen and O. Şahin, *J. Power Sources*, **195, 9** (2010) 2488-2495. DOI: 10.1016/j.jpowsour.2009.11.077
[103] G. Kim, N. Lee, K.-B. Kim, B.-K. Kim, H. Chang, S.-J. Song and J.-Y. Park, *Int. J. Hydrogen Energy*, **38, 3** (2013) 1571-1587. DOI: 10.1016/j.ijhydene.2012.11.044
[104] L.M. Kolchina, N.V. Lyskov, A.N. Kuznetsov, S.M. Kazakov, M.Z. Galin, A. Meledin, A.M. Abakumov, S.I. Bredikhin, G.N. Mazo and E.V. Antipov, *RSC Advances*, **6, 103** (2016) 101029-101037. DOI: 10.1039/c6ra21970e
[105] N.T. Hart, N.P. Brandon, M.J. Day and J.E. Shemilt, *Journal of Materials Science*, **36, 5** (2001) 1077-1085. DOI: 10.1023/a:1004857104328
[106] R. Pelosato, G. Cordaro, D. Stucchi, C. Cristiani and G. Dotelli, *J. Power Sources*, **298,** (2015) 46-67. DOI: 10.1016/j.jpowsour.2015.08.034
[107] Y.N. Kim, J.H. Kim and A. Manthiram, *J. Power Sources*, **195, 19** (2010) 6411-6419. DOI: 10.1016/j.jpowsour.2010.03.100
[108] J.C. Pérez-Flores, A. Gómez-Pérez, M. Yuste, J. Canales-Vázquez, E. Climent-Pascual, C. Ritter, M.T. Azcondo, U. Amador and F. García-Alvarado, *Int. J. Hydrogen Energy*, **39, 10** (2014) 5440-5450. DOI: 10.1016/j.ijhydene.2014.01.058

[109] K. Park, J. Kim and J. Bae, *Solid State Ionics*, **272,** (2015) 45-52. DOI: 10.1016/j.ssi.2014.12.014
[110] L. Fan, L. Liu, Y. Wang, H. Huo and Y. Xiong, *Ceram. Int.*, **40, 3** (2014) 4939-4944. DOI: 10.1016/j.ceramint.2013.10.088
[111] W. Li, J. Pu, B. Chi and L. Jian, *Electrochim. Acta*, **141,** (2014) 189-194. DOI: 10.1016/j.electacta.2014.07.021
[112] N.A. Danilov, A.P. Tarutin, J.G. Lyagaeva, E.Y. Pikalova, A.A. Murashkina, D.A. Medvedev, M.V. Patrakeev and A.K. Demin, *Ceram. Int.*, **43, 17** (2017) 15418-15423. DOI: 10.1016/j.ceramint.2017.08.083
[113] S. Duran, J. Tellez, M.V. Sandoval, M.A. Macias, E. Capoen, C. Pirovano, P. Roussel, A. Niemczyk, M. Barrera Castillo, L. Mogni, L. Suescun and G.H. Gauthier, *Solid State Ionics*, **326,** (2018) 116-123. DOI: 10.1016/j.ssi.2018.10.001
[114] S.B. Adler, *Chem. Rev.*, **104,** (2004) 4791-4843.
[115] M.G.H.M. Hendriks, J.E. ten Elshof, H.J.M. Bouwmeester and H. Verweij, *Solid State Ionics*, **146, 3** (2002) 211-217. DOI: https://doi.org/10.1016/S0167-2738(01)01017-7
[116] S. Gewies and W.G. Bessler, *J. Electrochem. Soc.*, **155, 9** (2008) B937-B952. DOI: 10.1149/1.2943411
[117] S. Pang, X. Jiang, X. Li, Q. Wang and Z. Su, *J. Power Sources*, **204,** (2012) 53-59. DOI: 10.1016/j.jpowsour.2012.01.034
[118] K. Yi, L. Sun, Q. Li, T. Xia, L. Huo, H. Zhao, J. Li, Z. Lü, J.-M. Bassat, A. Rougier, S. Fourcade and J.-C. Grenier, *Int. J. Hydrogen Energy*, **41, 24** (2016) 10228-10238. DOI: 10.1016/j.ijhydene.2016.04.248
[119] R. Pelosato, A. Donazzi, G. Dotelli, C. Cristiani, I. Natali Sora and M. Mariani, *J. Eur. Ceram. Soc.*, **34, 16** (2014) 4257-4272. DOI: 10.1016/j.jeurceramsoc.2014.07.005
[120] D. Chen, R. Ran, K. Zhang, J. Wang and Z. Shao, *J. Power Sources*, **188, 1** (2009) 96-105. DOI: 10.1016/j.jpowsour.2008.11.045
[121] R. Amin and K. Karan, *J. Electrochem. Soc.*, **157, 2** (2010) B285-B291. DOI: 10.1149/1.3267879
[122] M.J. Escudero, A. Aguadero, J.A. Alonso and L. Daza, *J. Electroanal. Chem.*, **611, 1–2** (2007) 107-116. DOI: http://dx.doi.org/10.1016/j.jelechem.2007.08.006

Declarations of interest: none